Passive scalar mixing in jets in crossflow

Suman Muppidi[*] and Krishnan Mahesh[†]

University of Minnesota, Minneapolis, MN, 55455, USA

Direct numerical simulations are used to study passive scalar transport and mixing in a round turbulent jet in a laminar crossflow. The velocity ratio of the jet to that of the crossflow is 5.7, the Schmidt number of the scalar is 1.49, and the jet–exit Reynolds number is 5000. The scalar field is used to compute entrainment of the crossflow fluid by the jet. It is shown that a bulk of this entrainment occurs on the downstream side of the jet. Also, the jet entrains a lot more than a simple jet even when the CVP is not yet formed and the jet has not yet bent into the crossflow. The reasons for a transverse jet's enhanced entrainment can be explained in terms of the pressure field around the jet. While the pressure gradient on the upstream side of the jet acts to bend it in the direction of the crossflow, the deformation of the jet's downstream side sets up a strong pressure gradient, that drives crossflow fluid toward the jet, resulting in increased entrainment.

I.   Introduction

A jet in crossflow, or a transverse jet, is a flow field where a jet of fluid enters and interacts with a crossflowing fluid. Practical examples of jets in crossflow include fuel injectors, smokestacks, film cooling on turbine blades and dilution holes in gas turbine combustors. A comprehensive review of past work on this problem is provided by Margason (1993). The emphasis has been on the study of the velocity and vorticity fields (Kamotani & Greber 1972, Fearn & Weston 1974, Andreopoulos & Rodi 1985, Fric & Roshko 1994, Krothapalli *et al.* 1990, Kelso *et al.* 1996), study of the scalar field and mixing (Smith & Mungal 1998, Shan & Dimotakis 2000, Su & Mungal 2004) and attempts at modeling the flow field and jet trajectory (Broadwell & Breidenthal 1984, Karagozian 1986, Hasselbrink & Mungal 2001, Muppidi & Mahesh 2005a).

Some of the recent work on jets in crossflow involves numerical simulations. Chochua *et al.* (2000) performed RANS calculations and compared their results to experiments (UTRC). Though their simulations predicted the mean velocities reasonably, their turbulent intensities showed significant differences from those of the experiment. Yuan *et al.*(1999) performed LES of a round jet in crossflow and showed reasonable agreement for mean velocities and turbulent intensities with experimental results of Sherif & Pletcher (1989). Schluter & Schonfeld (2000) compared the results of their LES with experimental velocity profiles of Andreopoulos & Rodi (1984) and scalar fields of Smith & Mungal (1998), and obtained reasonable agreement. Velocity and turbulent intensity profiles from DNS of a turbulent jet in crossflow by Muppidi & Mahesh (2005b) agree well with experimental results of Su & Mungal (2004).

Su & Mungal (2004) note that even though a number of applications of jets in crossflow involve mixing, the body of work devoted to mixing of jets in crossflow is relatively small. The results from their experiments were used to provide a comprehensive view of the scalar field. Some studies credit the counter–rotating vortex pair (CVP) for the enhanced mixing observed in transverse jets, as compared to regular jets. Smith & Mungal (1998) show that the scalar centerline decay is faster in the near field as compared to that in the far field. They conclude that in the near field, the CVP itself does not enhance mixing. By studying the PDFs of scalar concentration, Shan & Dimotakis (2001) find that an increase in Reynolds number enhances mixing.

The objective of the present paper is to study passive scalar transport and mixing characteristics in a round turbulent transverse jet, using DNS. The simulations are performed at conditions corresponding to the experiment

---

[*]Graduate Research Assistant
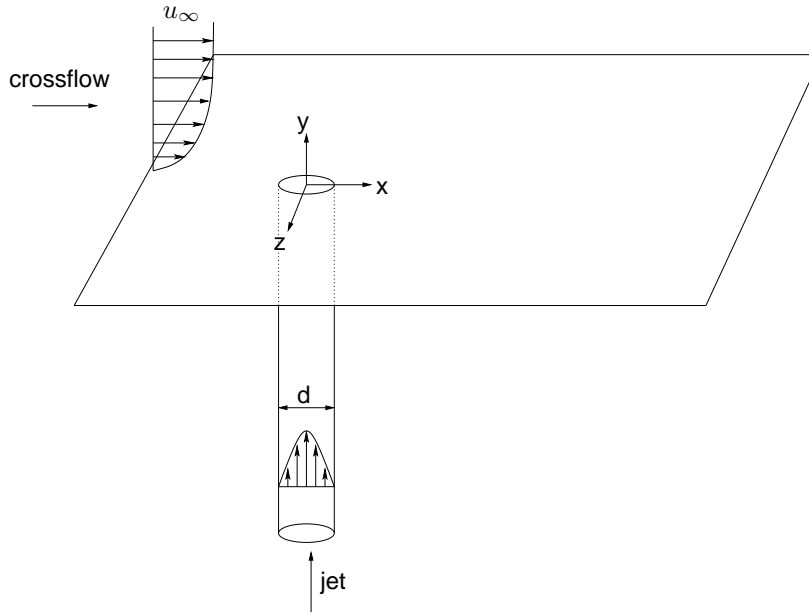
[†]Associate Professor

Figure 1. Schematic of the problem.

by Su & Mungal. This paper is organized as follows. The simulation details are presented in section II – the problem is described in subsection A, and the numerical details are briefly mentioned in subsections B and C. Section III contains the results of the simulation. Some characteristic features of the scalar field are presented in subsection A. The scalar field is used to examine how the jet entrains crossflow fluid in section III B, which also relates the dominant entrainment mechanisms to the pressure field.

II.   Simulation details

A brief description of the problem, algorithm, and numerical details are presented in this section. Detailed description of the algorithm is available in Mahesh *et al.* (2004), and that of the numerical details for this problem – computational domain, computational mesh, boundary conditions *etc.* are available in Muppidi & Mahesh (2005b).

A.   Problem

A schematic of the problem is shown in figure 1. The jet issues perpendicularly from a round pipe into the crossflow. The crossflow and the jet are in the x–direction and y–direction respectively. The velocity ratio, used to characterize a jet in crossflow is defined as $r = \overline{u}_j/u_\infty$, where $\overline{u}_j$ is the mean jet velocity, and u_∞ is the freestream crossflow velocity. Conditions of the simulation are similar to an experiment by Su & Mungal (2004). The velocity ratio is 5.7 and the Reynolds number of the flow (Re $= u_j d/\nu$) is 5000. The jet is fully turbulent and the crossflow is laminar (with a boundary layer thickness $\delta_{80\%} = 1.32d$ at the location of the jet–exit, in the absence of the jet). In the experiment, the jet fluid is seeded with acetone vapour. This gives a density ratio $\rho_j/\rho_\infty = 1.1$, and a Schmidt number $Sc= 1.49$. In the present simulations, the densities of the jet and crossflow fluids are taken to be the same, and the passive scalar computation is performed at the same Schmidt number as in the experiment.

B.   Algorithm

The simulations are performed using an algorithm that solves the incompressible Navier–Stokes equations

$$\frac{\partial u_i}{\partial t} + \frac{\partial u_i u_j}{\partial x_j} = -\frac{\partial p}{\partial x_i} + \nu \frac{\partial^2 u_i}{\partial x_j x_j} \ , \quad \frac{\partial u_i}{\partial x_i} = 0 \tag{1}$$

American Institute of Aeronautics and Astronautics Paper 2006-1098
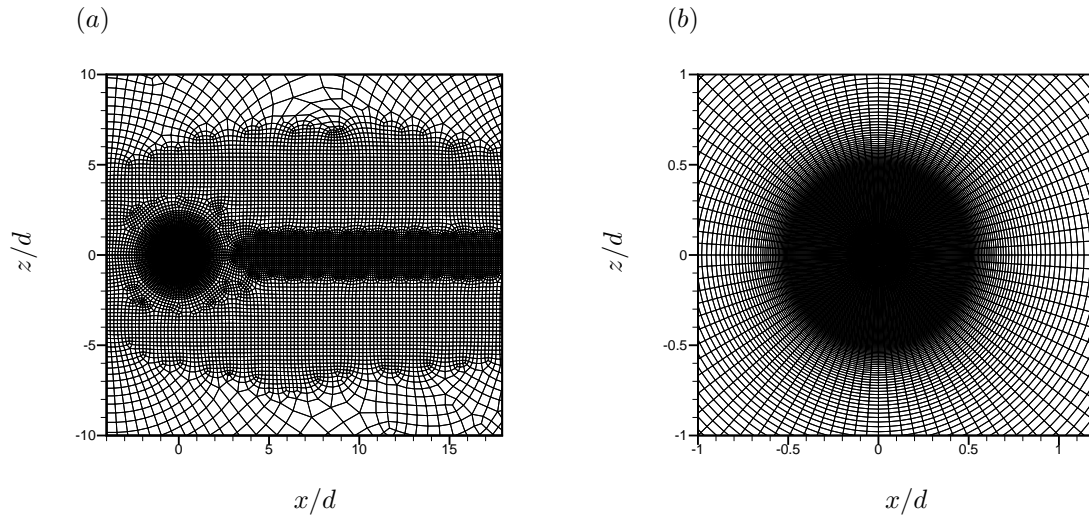
(a) (b)

Figure 2. (a) **Horizontal slice of the computational mesh shows the elements in the region around the jet–exit and on the symmetry plane where the profiles are compared. Shown is only a part of the domain.** (b) **Computational mesh in the vicinity of the jet–exit shows the elements in greater detail.**

on unstructured grids. Here u_i, p and ν denote the velocities, pressure and kinematic viscosity respectively. The density of the fluid is constant, and is absorbed into the pressure. The numerical scheme is described in detail in Mahesh *et al.* (2004). The algorithm is a predictor–corrector formulation and emphasizes discrete energy conservation on unstructured grids. This property makes the computations robust at high Reynolds numbers without numerical dissipation. The velocity and pressure fields are stored at the control volume centroids, and are integrated in time implicitly using a Crank–Nicholson scheme.

The passive scalar is computed by solving the advection–diffusion equation

$$\frac{\partial C}{\partial t} + \frac{\partial C u_j}{\partial x_j} = \frac{\nu}{Sc}\frac{\partial^2 u_i}{\partial x_j x_j} \ , \tag{2}$$

where C is the concentration of the scalar. The jet fluid has a value of $C = 1.0$, and the crossflow fluid has $C = 0.0$. The spatial derivatives are computed using a predictor–corrector method. First the scalar field is advanced using a second–order central difference scheme. This predicted scalar field is corrected in regions of scalar overshoot using a first order upwind scheme. This corrector step ensures that locally, the passive scalar concentration is bounded (*i.e.* $C \in [0,1]$), and is based on the work by Herrman *at al.* (2004). The scalar is advanced in time explicitly using RK4 scheme in an inner loop.

C.   Computational Domain and Boundary Conditions

The computational domain extends $32d \times 64d \times 64d$ in the axial, wall-normal and spanwise directions (x, y and z) respectively, and includes a $2d$ length of the pipe. Preliminary computations showed that a domain of this size does not constrain the jet, and the flow does not feel the effects of confinement by the boundary. The crossflow inflow plane is located $4d$ upstream of the jet–exit.

The crossflow is modeled as a laminar flow past a flat plate (Schlichting 1968). Based on the analytical solution to the Blasius boundary layer, a velocity field is specified at the inflow plane of the crossflow such that in the absence of the jet, the crossflow has the prescribed $\delta_{80\%}$ at the center of the jet–exit. In order to simulate a fully turbulent jet, a separate simulation of fully developed turbulent flow in a pipe is performed. The Reynolds number for this computation, based on the pipe diameter and the mean axial velocity, is 5000. The velocity field at a cross–section (normal to the pipe axis) from this simulation is stored over a length of time, and input at the inflow plane of the pipe as the time–dependent boundary condition for the jet in the present simulation. The crossflow boundary condition is validated by comparing velocities with the similarity solution and the jet boundary condition is validated by comparing with existing results of Eggels *et al.* (1994). Both these validations are shown in Muppidi & Mahesh (2005b). On the exit plane ($x/d = 32$), a zero–gradient boundary condition is
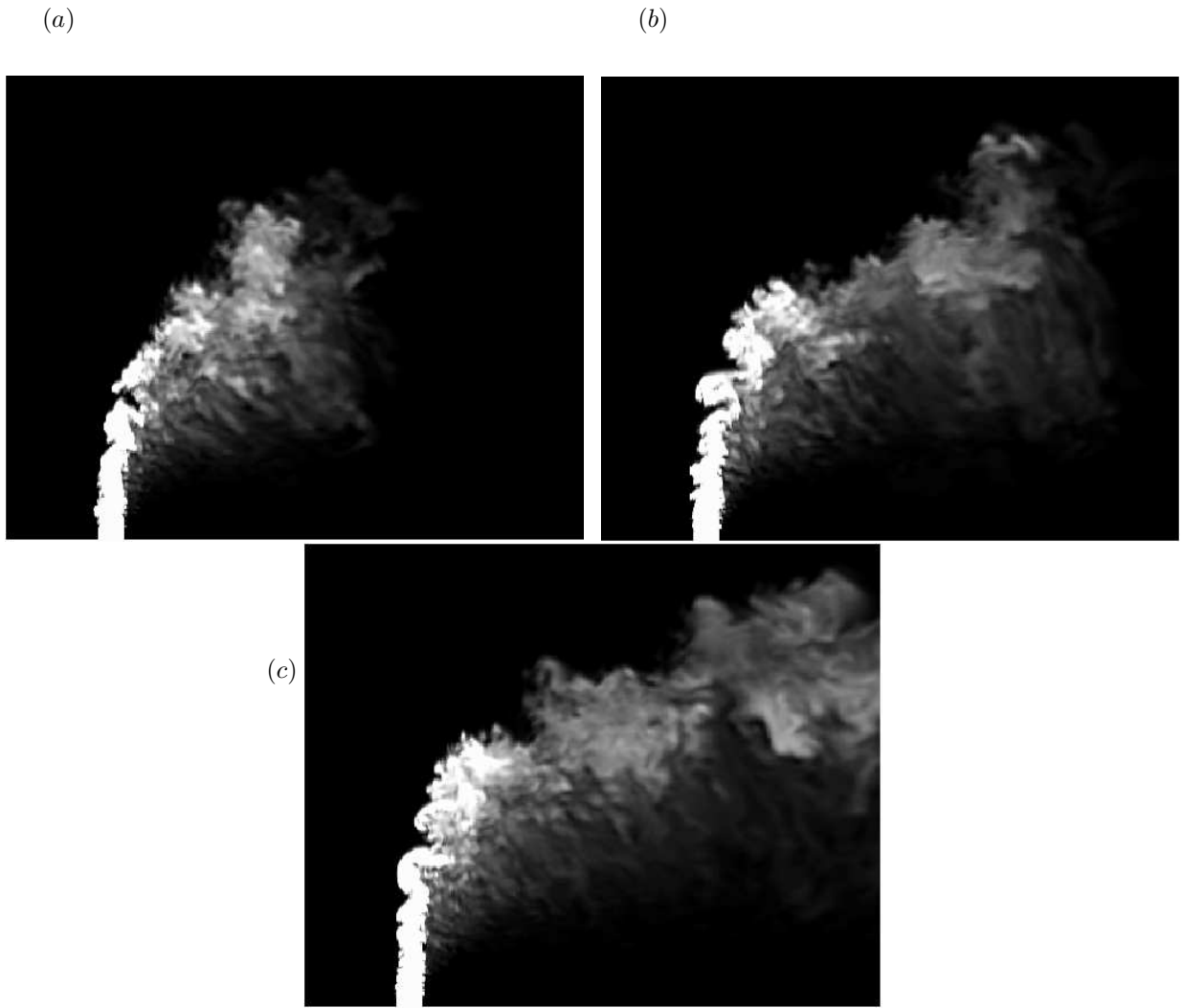
Figure 3. Instantaneous contours of passive scalar on the symmetry plane at different time instants after the scalar has been introduced into the flow.

used for the velocities. On the spanwise boundaries ($z/d = \pm\, 32$), the velocity field corresponding to the laminar crossflow is specified. Freestream velocity boundary conditions are specified on the top boundary ($y/d = 64$).

The computational mesh is unstructured and consists of approximately 11 million hexahedral elements. A representative slice of the mesh is shown in figure 2(a). As the coordinates indicate, the direction of the crossflow is from left to the right, and the jet fluid travels into the plane of this figure. The finest elements are found at the walls of the pipe and of the crossflow. The largest elements are found away from the jet–exit and away from the wall.

III.   Results

The velocity field was compared with profiles of the mean jet trajectory, mean velocity and turbulent intensities available from the experiment. These comparisons were presented in Muppidi & Mahesh (2005b) and show a reasonable agreement. In order to account for the density ratio in the experiments, profiles were scaled using the effective velocity ratio $r_{eff} = \frac{\rho_j u_j^2}{\rho_\infty u_\infty^2}$.
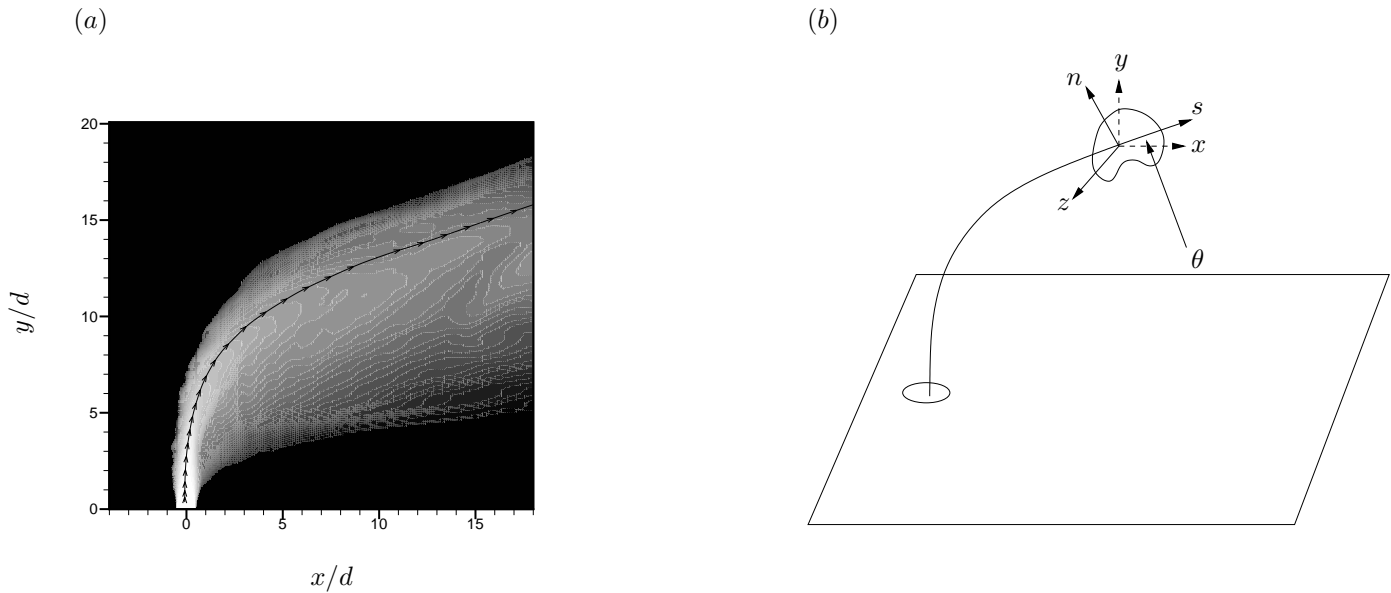
American Institute of Aeronautics and Astronautics Paper 2006-1098

Figure 4. (a) Time–averaged contours of passive scalar concentration on the symmetry plane. Also shown is the mean center streamline, indicating the jet trajectory. (b) Schematic of the coordinate system that is aligned with the jet trajectory.

A. Scalar field

Figure 3 shows the instantaneous contours of passive scalar concentration on the symmetry plane. These figures correspond to different time instants after the scalar has been introduced along with the jet fluid. Note that the scalar is introduced only after the velocity field is considered statistically stationary and, hence, these figures represent the 'physical' solution, and not a 'transient' stage of the solution.

On the downstream side of the jet, we observe 'fingers' or 'filaments' of jet fluid reaching into the crossflow fluid, normal to the jet trajectory. Similar fingers were observed by Shan & Dimotakis (2001) and Su & Mungal (2004), who suggest that these filaments likely correspond to the wake vortices. Fric & Roshko (1994), however, show that the wake vortices are observed only when the crossflow fluid is seeded, and not when the jet fluid is seeded. These filaments exist very close to the symmetry plane, are observed on the symmetry plane and end view planes, and are virtually non–existent on off–symmetry planes. The present results are in agreement with that reported by Su & Mungal.

Contours of time–averaged scalar concentration on the symmetry plane are shown in figure 4(a). Also shown is the center streamline, indicating the mean jet trajectory. Figure shows that the scalar concentration decreases with increasing distance from the jet–exit. Also, the jet width is larger on the downstream side as compared to the upstream side of the center streamline. Qualitatively, figures 3(c) and 4(a) are similar to those available from the experiment.

Jet width can be quantitatively studied by plotting the scalar concentration in the trajectory–normal direction, in a trajectory based coordinate system. This coordinate system is shown in figure 4(b). At any point along the jet trajectory, s is the distance from the jet–exit, along the center streamline. n is the coordinate normal to the trajectory. The s–n plane is the same as the x–y plane, and the z coordinate is the same in both the coordinate systems. Figure 5(a) shows the variation of the mean scalar concentration with n. The curves correspond to different downstream distances. At any s, n=0 corresponds to the point where the center streamline crosses the z–n plane.

At the location s=d, the peak scalar concentration is C_0 across almost the entire jet edge. Past the jet edge, both downstream and upstream, the fluid contains no scalar, and the gradients near the jet edge are sharp. At the next location, $s = 3d$, the peak scalar concentration is lower than C_0 and corresponds to $n = 0$. On the upstream side, there is no scalar present past the leading edge of the jet. On the downstream side, in contrast, a small amount of scalar is observed up to a distance of about 2.5 d past from the jet centerline. Clearly – if the jet width were defined based on a cutoff scalar concentration ($C/C_0 = 0.1$, say) – at this location, the jet width
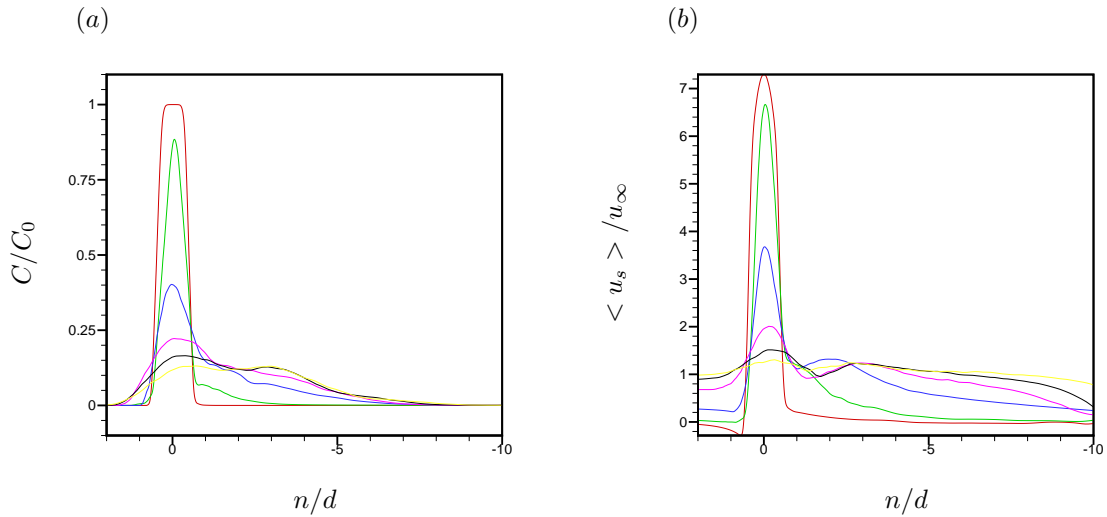
Figure 5. (*a*) **Variation of mean scalar concentration along the trajectory–normal variable** n. **The profiles correspond to** $s = d$ **(red),** $3d$ **(green),** $6d$ **(blue),** $9d$ **(pink),** $12d$ **(black) and** $15d$ **(yellow).** (*b*) **Variation of velocity** $< u_s >$ **at the same locations.**

downstream of the center streamline is greater than that upstream. Moving further, this trend continues : peak C decreases and the jet width on the downstream side increases. By $s=12d$, the peak scalar concentration is not that much greater compared to the scalar concentration across the jet width, resulting in a 'plateau' shaped profile.

In the s–n–z coordinate system, fluid velocities can be represented in terms of trajectory–based components u_s, u_n and w by a simple coordinate transformation. Figure 5(b) shows the profiles of time–averaged velocity u_s against n. The profiles correspond to the same locations as those in figure 5(a). A few similarities can be observed by contrasting figures 5(a) and 5(b). At $s=d$, peak u_s is observed at the center of the jet. There is a negative velocity region just upstream of the jet, and past the downstream edge, magnitude of u_s is very low. At $s=3d$, the peak velocity decreases, as the jet fluid decelerates. Unlike at $s=d$, considerable fluid velocity u_s is observed up to about $4d$ downstream of the jet centerline. Qualitatively, this is very similar to the scalar profile at $s=3d$ in figure 5(a).

Figure 6 compares profiles of the mean scalar concentration obtained from the present simulation, with that from the experiment. These profiles correspond to the symmetry plane, and to three vertical locations : $y = 0.1rd$, $0.5rd$, and $1.0rd$. The agreement appears reasonable at the first two locations, while there is some deviation between the simulation and the experiment at $y = rd$. To obtain these profiles, statistics were compiled over a $16d/u_\infty$ length of time. At the farthest station, the time scales of the flow are significantly smaller as compared to the first two stations. For example, peak velocity magnitude ($u_m = \sqrt{u^2 + v^2}$) decreases by a factor of over 2 between $y=0.1rd$ and $y=1.0rd$. We believe that the statistics have not converged at the farthest station, and also that with statistically converged data, the deviation would decrease. More samples are being gathered.

B.   Entrainment

Entrainment of the crossflow fluid by the jet fluid is computed using the volume flux across the trajectory–normal planes. A threshold value for the scalar concentration allows differentiation between the crossflow fluid and the scalar–containing jet fluid. Figure 7(a) shows the volume flux (normalized by that at the jet–exit) as a function of the distance from the jet–exit. The figure also shows the Ricou–Spalding correlation (Ricou & Spalding 1961) for the volume flux in a free jet, which states that entrainment increases linearly with distance from the jet–exit. Figure 7(a) shows that entrainment in the transverse jet is significantly larger as compared to that in a free jet. A similar result has been shown by Yuan & Street (1998). Entrainment in a transverse jet is about twice that in a free jet at a distance $6d$ and at a distance $9d$, it is about three times as much. At the jet–exit, $s=0$, and $V_s = V_0$. This, of course, is also true for a regular jet. At a distance d, a free jet's entrainment is in fact greater than that of the jet in crossflow. At a distance of 2 diameters downstream, the entrainment appears same for both. There after, the transverse jet's entrainment increases acutely.
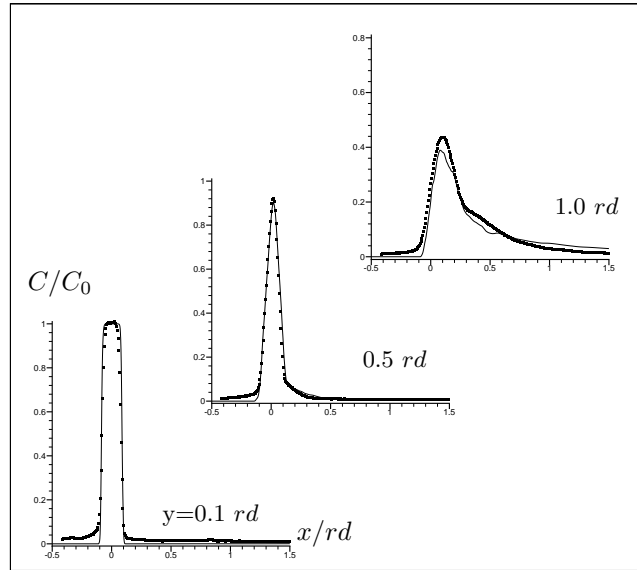
American Institute of Aeronautics and Astronautics Paper 2006-1098

Figure 6. Comparison of mean scalar concentration profiles. Lines show results from the present simulation. Symbols show results from experiment.

1. Entrainment Mechanism

Close to the jet–exit, the jet is vertical and the entrainment characteristics would be expected to be similar to that of a simple jet, which is indeed seen in figure 7(a). It has been proposed (Yuan & Street 1998) that in the highly curved part of the jet's trajectory, entrainment is enhanced on the upstream face of the jet due to the high angle of incidence between the jet and crossflow velocities. The jet in the present simulations is fairly vertical until past 5 diameters past the jet–exit. At $s = 2d$, the angle of the jet trajectory is $88°$ with the streamwise direction. Even at $4d$, the angle is $80.9°$. The angles at $6d$, $8d$ and $10d$ are $71.5°$, $56.4°$ and $44.5°$ respectively. The sharp increase in the entrainment, hence, cannot be a consequence of the bending of the jet. To further study the effectiveness of the upstream side of the jet in entraining crossflow fluid, entrainment on the upstream and downstream sides of the jet are computed separately. Figure 7(b) shows the percentage contribution of the downstream side of the jet to the total entrainment. Close to the jet–exit, both the downstream and upstream sides of the jet contribute about the same to the total entrainment, and in this region, the transverse jet's entrainment is roughly same as that of a simple jet, as observed in figure 7(a). Moving further, the contribution of the downstream side increases significantly. For example, at a distance of $6d$ from the jet–exit, the upstream side contributes to only about 10% of the total entrainment. It appears that the increased entrainment past $2d$ roughly corresponds to the increased contribution of the downstream side of the jet to the total entrainment.

The CVP has been considered responsible for most of the entrainment observed in the far field. Yuan & Street (1998) propose that the CVP increases the surface area of the jet, enabling increased entrainment. Smith & Mungal (1998) indicate that it is the process of CVP formation, and not the CVP itself, that enhances mixing in the near field. Results from the present simulation show that it takes a few diameters for the jet cross–section to deform and for the CVP to be fully formed. The increased entrainment in the near–field is not an effect of the CVP. Figures 7(a) and (b) plot the entrainment rates up to a distance of $s=10d$ ($x \sim 3d$ & $y \sim 9.2d$) and are not sufficient to comment upon the role of the CVP in affecting entrainment characteristics in the far–field.

The question remains : what *does* enhance entrainment in a transverse jet ? Figure 7(c) shows the time–averaged streamlines on the symmetry plane. Streamlines emanating from the leading and trailing edges of the jet–exit indicate the jet boundary. Other streamlines indicate the motion of the crossflow fluid. Streamlines entering the domain from the crossflow boundary, upstream of the jet, appear to bend in the direction of the jet fluid – and almost merge with the leading edge boundary of the jet. These streamlines must account for the upstream side entrainment of the jet. In addition, the jet entrains fluid on the downstream side, and the source of this entrainment is the *node* observed in the vicinity of the coordinate $x \sim 2.5\,d$, $y \sim 1.8\,d$. The presence of this node has been well–documented (*e.g.* Kelso *et al.* 1996). The local flow field acts as a source in the symmetry
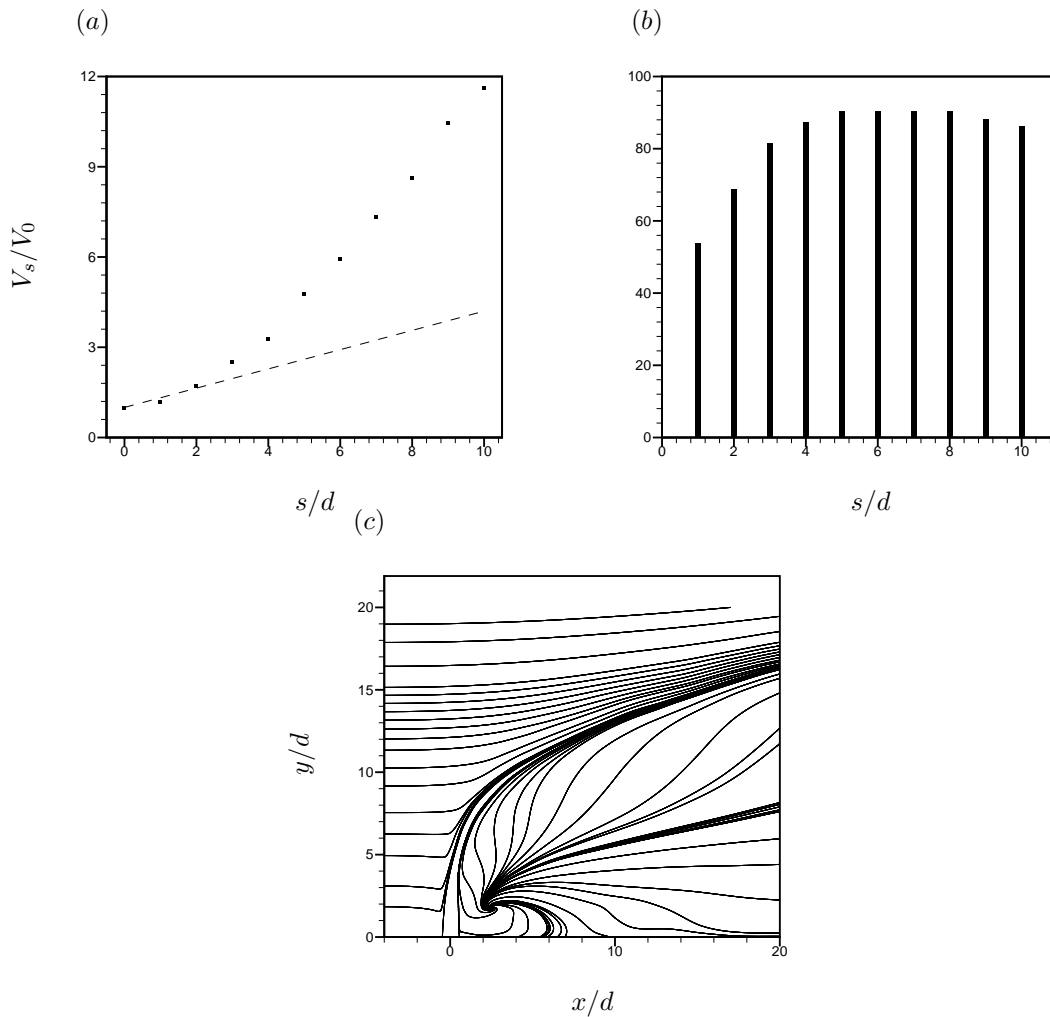
American Institute of Aeronautics and Astronautics Paper 2006-1098

(a)

(b)

(c)

Figure 7. (*a*) **Volume flux of the scalar carrying fluid plotted along the length of the jet.** ---- **shows Ricou–Spalding correlation for entrainment in a simple jet.** (*b*) **Percentage contribution of the downstream side of the jet, to the total entrainment, plotted as a function of the jet length.** (*c*) **Mean streamlines on the symmetry plane.**

plane (note the streamlines fanning out across the plane) and a sink in the horizontal plane (the streamlines pass *around* the jet and converge toward this node). Due to this dual behavior, this point is sometimes termed the 'saddle-node'. The intensity of this (downstream side) entrainment is high, as can be seen by the steep angle of the streamlines toward the jet's downstream boundary.

Entrainment by free jets is commonly attributed to the coherent motions at the edges of the jet. In the case of transverse jets, the flow field causes more crossflow fluid to come into contact with the jet fluid on the downstream side. This, in turn, results in the downstream side of the jet entraining more fluid than the upstream side, causing much higher entrainment than observed in a regular jet. An explanation of this phenomenon, in terms of the pressure field downstream of the jet, follows.

2. Entrainment explained in terms of the downstream pressure field

Figure 8(a) shows the contours of mean pressure on the symmetry plane along with a few characteristic in–plane streamlines (shown in green). The highest pressure on this plane is observed near the upstream edge of the jet, beginning close to the jet–exit/wall and extending until the jet noticeably bends. The lowest pressure is observed near the downstream edge of the jet (at about $y \sim 5d$). Moving in the x–direction, the pressure begins to increase past the downstream edge. The vectors in figure 8(a) show the quantity $-\nabla p$ on the symmetry plane. The direction of the vectors downstream of the jet shows that the pressure gradient drives crossflow fluid toward
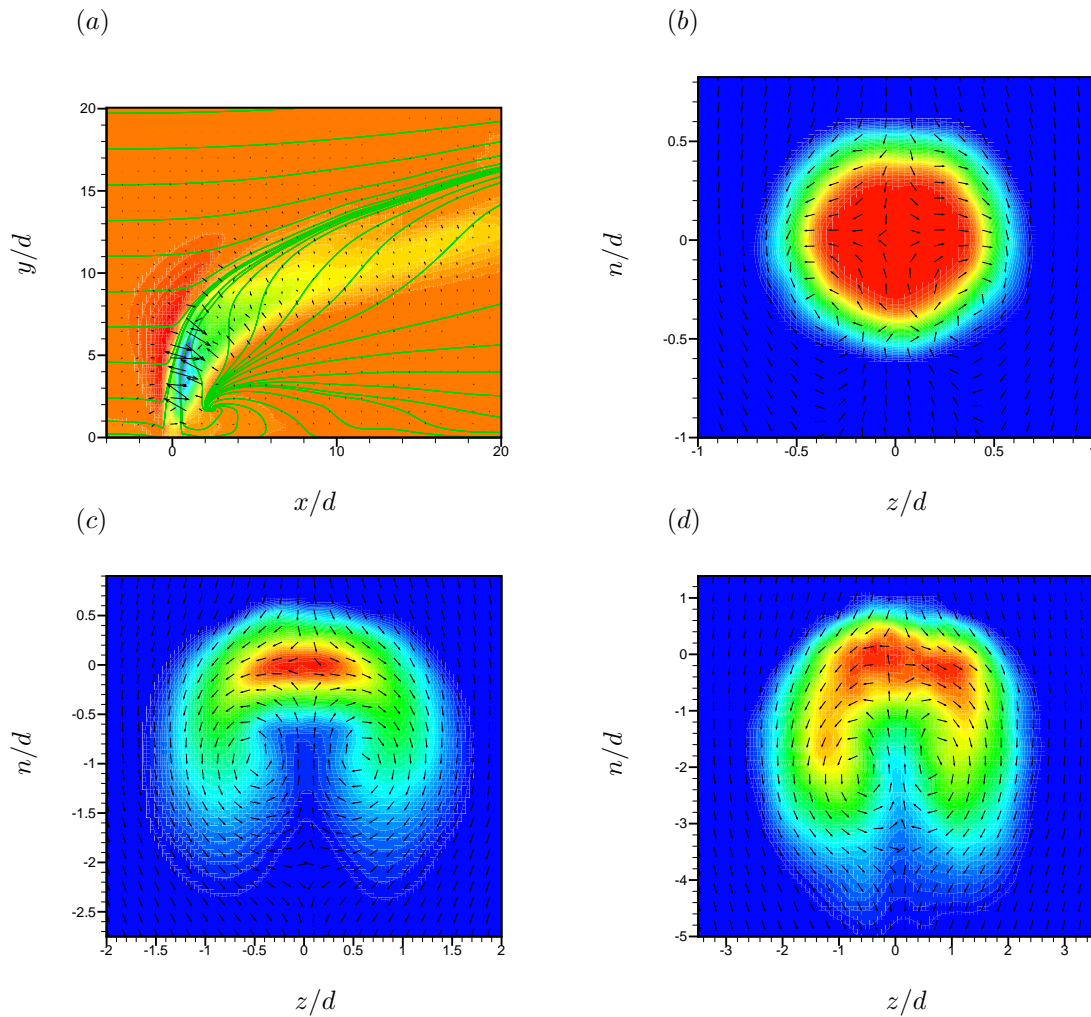
American Institute of Aeronautics and Astronautics Paper 2006-1098

Figure 8. (*a*) **Contours of pressure on the symmetry plane along with in–plane streamlines (in green). The black vectors indicate the quantity** $-\nabla p$ **on the symmetry plane.** (*b*) **Jet cross–section at** $s{=}d$**. Contours of scalar along with in–plane velocity vectors.** (*c*) **Jet cross–section at** $s = 4d$**, scalar contours, in–plane velocity vectors, and** (*d*) **Jet cross–section at** $s = 7d$**, scalar contours, in–plane velocity vectors.**

the jet. The magnitude of these pressure gradients is significant, as evident from the length of the vectors. This pressure field causes large amounts of crossflow fluid to come into contact with the jet fluid, enabling it to be entrained. The presence of the saddle–node, acting as a source, in this region of high pressure gradients further enhances crossflow entrainment on the downstream side.

Figures 8(b) – 8(d) show the jet cross–section on the trajectory–normal plane. Contours of time–averaged scalar concentration are shown, along with in–plane velocity vectors. The three cross–sections correspond to downstream distances of d, $4d$ and $7d$ respectively. The jet is barely deformed at $s = d$ and though the jet cross–section is deformed at $s = 4d$, the CVP is not completely formed. The velocity vectors show the motion of crossflow fluid, downstream of the jet's trailing edge, toward the trailing edge – indicating entrainment on the downstream side.

There is a need to differentiate between the $-\nabla p$ vectors near the leading edge of the jet (pointing in the $+ve$ x, $+ve$ y direction) and those downstream of the jet's trailing edge (pointing in the $-ve$ x, $+ve$ y direction). The high pressure region upstream of the jet's leading edge occurs very close to the leading edge and follows it. Very few vectors of considerable magnitude originate in the freestream crossflow fluid. Hence, the pressure gradient in this region does not affect the upstream entrainment. On the downstream side, however, the high pressure region and the resulting pressure gradients are observed at a distance from the jet's trailing edge (as far as about $4d$ away, at $s \sim 6d$) and more than a few vectors of considerable magnitude are observed to originate in
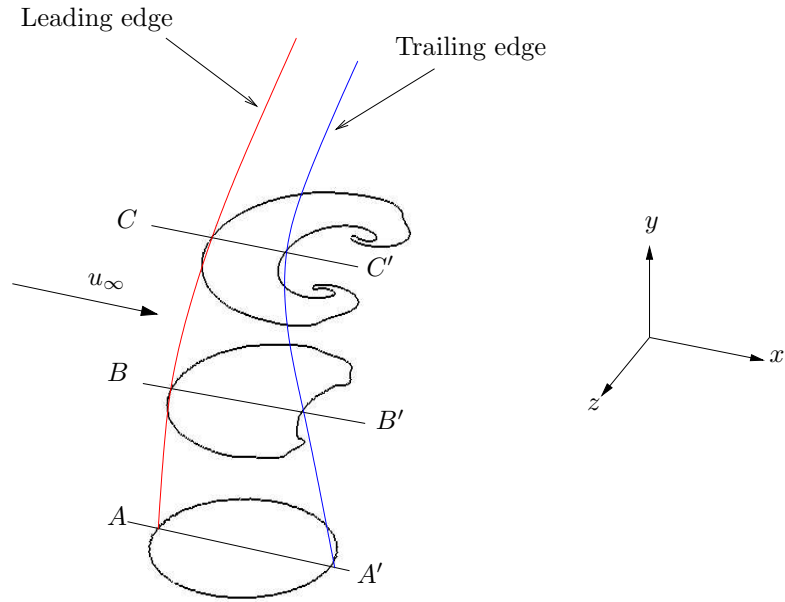
Figure 9. Schematic of the near–field of the jet.

the downstream crossflow fluid. Hence, the pressure field upstream of the jet acts to bend the jet in the direction of the crossflow while the pressure gradient downstream of the jet acts to enhance entrainment.

Figure 9 shows a schematic of the jet in the near–field of the jet–exit. The crossflow is in the x–direction and the direction of the jet is along the y–axis. Cross–sections of the jet at three distances from the wall are shown, corresponding to planes A–A', B–B' and C–C'. Section A–A' is very close to the jet–exit and section C–C' is the point where after the jet begins to bend significantly into the crossflow. At A–A', the jet cross–section is roughly circular, and corresponds to figure 8(b) from the simulation. The jet fluid has a high velocity (as compared to u_∞) and momentum, and the crossflow fluid sees it as an obstacle. Crossflow fluid (on the symmetry plane) decelerates just upstream of the jet, and there is a high pressure region as observed in figure 8(a). The figure also shows a high pressure region just downstream of the trailing edge. The jet fluid has no velocity in the x–direction and is subject to an acceleration in that direction, due to the crossflow fluid. Muppidi & Mahesh (2005c) showed, using a model problem, that the opposing directions of the pressure gradient and the acceleration on the trailing edge of the jet cause the trailing edge to move closer to the leading edge, deforming the jet from a circular cross–section to a kidney–shaped cross–section. Sections B–B' and C–C' in figure 9 show stages of deformation of the jet cross–section. This change in cross–section is also evident in figures 8(c) and (d). As the jet evolves (between A–A' and C–C'), note that the leading edge accelerates, and moves, in the direction of the crossflow, while the trailing edge moves closer to the leading edge. This deformation of the jet causes the trailing edge pressure to decrease. Crossflow fluid downstream of the trailing edge, however, has a higher pressure and this pressure gradient drives crossflow fluid toward the trailing edge, enhancing entrainment on the downstream side.

IV.   Summary

Direct numerical simulation of passive scalar transport in a turbulent transverse jet is performed. The conditions of the simulation correspond to a recent experiment. The scalar field from the simulation appears qualitatively similar to the experimental results. Quantitative comparison of the mean scalar concentration profiles agree well in the near field while a difference is observed at greater distances from the jet–exit. This is a result of slower time scales in the far field and lack of statistical convergence in the present results. Increased mixing in the near–field of a jet in crossflow can be related to its enhanced entrainment as compared to a regular jet. It is observed that entrainment is significantly higher on the downstream side of the jet as compared to

the upstream side. The pressure gradient near the trailing edge of the jet–exit opposes the acceleration of the jet in the direction of the crossflow. This causes the cross–section to deform and the trailing edge pressure to decrease with increasing distance from the jet–exit. The resulting strong pressure gradient, along with the three dimensionality of the flow field, drives downstream crossflow fluid toward the jet, causing the increased entrainment, as observed.

Acknowledgments

References

[1] Andreopoulos, J. & Rodi, W. 1984 Experimental investigation of jets in a crossflow *J. Fluid Mech.* **138:** 93–127.

[2] Broadwell, J.E. & Breidenthal, R.E. 1984 Structure and mixing of a transverse jet in incompressible flow *J. Fluid Mech.* **148:** 405–412.

[3] Chochua, G., Shyy, W., Thakur, S., Brankovic, A., Lienau, K., Porter, L. & Lischinsky, D. 2000 A computational and experimental investigation of turbulent jet and crossflow interaction. *Numer. Heat Transfer, Part A.* **38:** 557–572.

[4] Eggels, J.G.M., Unger, F., Weiss, M.H., Westerweel, J., Adrian, R.J., Friedrich, R. & Nieuwstadt, T.M. 1994 Fully developed turbulent pipe flow : a comparison between numerical simulation and experiment. *J. Fluid Mech.* **268:** 175 –209.

[5] Fearn, R.L. & Weston, R.P. 1974 Vorticity associated with a jet in crossflow. *AIAA J.* **12:** 1666–1671.

[6] Fric, T.F. & Roshko, A. 1994 Vortical structure in the wake of a transverse jet *J, Fluid Mech.* **279:** 1–47.

[7] Hasselbrink, E.F & Mungal, M.G. 2001 Transverse jets and jet flames. Part 1. Scaling laws for strong transverse jets *J. Fluid Mech.* **443:** 1–25.

[8] Herrman, M., Blanquart, G. & Raman, V. 2004 Flux corrected finite–volume scheme for preserving scalar boundedness in large–eddy simulations. In *Annual Research Briefs - 2004*, pp. 75–85. Stanford, CA: Center for Turbulence Research.

[9] Karagozian, A.R. 1986 An analytical model for the vorticity associated with a transverse jet *AIAA J.* **24:** 429–436.

[10] Kamotani,Y. & Greber, I. 1972 Experiments on turbulent jet in a crossflow *AIAA J.* **10:** 1425 – 1429.

[11] Kelso, R.M., Lim, T.T & Perry, A.E. 1996 An experimental study of round jets in cross–flow. *J. Fluid Mech.* **306:** 111–144.

[12] Krothapalli, A., Lourenco,L. & Buchlin, J.M. 1990 Separated flow upstream of a jet in a crossflow *AIAA J.* **28:** 414–420.

[13] Mahesh, K., Constantinescu, G. & Moin, P. 2004 A numerical method for large–eddy simulation in complex geometries. *J. Comput. Phys.* **197:** 215–240.

[14] Margason, R.J. 1993 Fifty years of jet in crossflow research. In *AGARD Symp. on a jet in Cross Flow* Winchester, UK *AGARD CP*–534.

[15] Muppidi, S. & Mahesh, K. 2005a Study of trajectories of jets in crossflow using direct numerical simulations *J. Fluid. Mech.* **530:** 81 – 100.

[16] Muppidi, S. & Mahesh, K. 2005b Direct numerical simulation of turbulent jets in crossflow *AIAA* Paper 2005–1115.

[17] Muppidi, S.& Mahesh, K. 2005c Velocity field of a round turbulent transverse jet. In *Proc. 4th Int. Symp. on Turbulence and Shear Flow Phenomena* Williamsburg, Virginia, Paper *TSFP4-197* pp 829-834.

[18] Schlichting, H.T. 1963 Boundary Layer Theory, McGraw Hill.

[19] Schluter, J.U. & Schonfeld, T. 2000 LES of Jets in Crossflow and its Application to a Gas Turbine Burner *Flow Turbulence and Combustion* **65(2):** 177–203.

[20] Shan, J.W. & Dimotakis, P.E. 2001 Turbulent mixing in transverse jets *GALCIT FM:2001.006*.

[21] Sherif, S.A. and Pletcher, R.H. 1989 Measurements of the Thermal Characteristics of Heated Turbulent Jets in Cross Flow. *ASME J. Heat Transfer* **111:** 897–903.

[22] Smith, S.H. & Mungal, M.G. 1998 Mixing, structure and scaling of the jet in crossflow *J. Fluid Mech.* **357:** 83–122.

[23] Su, L.K. & Mungal, M.G. 2004 Simultaneous Measurement of Scalar and Velocity Field Evolution in Turbulent Crossflowing Jets *J. Fluid Mech.* **513:** 1–45.

[24] Yuan, L.L. & Street, R.L. 1998 Trajectory and entrainment of a round jet in crossflow *Phys. Fluids* **10:** 2323–2335.

[25] Yuan, L.L., Street, R.L. & Ferziger, J.H. 1999 Large–eddy simulations of a round jet in crossflow *J. Fluid Mech.* **379:** 71–104.